JACS
JOURNAL OF THE AMERICAN CHEMICAL SOCIETY
pubs.acs.org/JACS
Article

Genetically Encoded Sensor Enables Endogenous RNA Imaging with Conformation-Switching Induced Fluorogenic Proteins

Wen-Jing Zhou, Hua Li, Ke-Ke Zhang, Fenglin Wang,* Xia Chu, and Jian-Hui Jiang*

Cite This: *J. Am. Chem. Soc.* 2021, 143, 14394−14401

ABSTRACT: Genetically encoded molecular tools are crucial for live cell RNA imaging, and few are available for endogenous RNA imaging. We develop a new genetically encoded sensor using conformation switching RNA induced fluorogenic proteins that enable multicolor and signal-amplified imaging of endogenous RNAs. The sensor system is designed with an RNA sensing module and a degron-fused fluorescent protein reporter. Target RNA induces conformation switching of the RNA sensing module to form RNA aptamers that stabilize the degron-fused protein for fluorogenic imaging. This sensor is demonstrated for high-contrast imaging of *survivin* mRNA abundance and dynamics in live cells. Moreover, the sensor system is extended to a multicolor palette by screening fluorogenic proteins of distinct colors, and engineered into a signal amplifier using the split fluorescent protein design. The sensor is further exploited for imaging lncRNA MALAT-1 and its translocation dynamics during mitosis. Our sensor system can afford a valuable platform for RNA imaging in biomedical research and clinical theranostics.

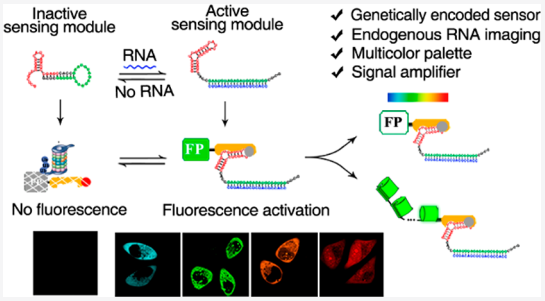

INTRODUCTION

RNAs including mRNAs, microRNAs, and long noncoding RNAs (lncRNAs) play essential roles in the regulation of various biological processes. The abundance and subcellular distribution of RNAs are tightly regulated, and abnormal expressions and localizations are implicated in the development of different diseases. Imaging and tracking of dynamics of RNA abundance and localization are crucial for understanding their cellular functions and providing insights for disease theranostics.[1] Traditional methods for imaging of RNA dynamics rely on two major strategies, fluorescent protein tagged RNA binding proteins[2,3] or DNA-based hybridization probes.[4−6] However, these methods suffer from limitations such as high background from excessively expressed fluorescent protein fusions or difficulties in efficient biological delivery.

Emerging genetically encoded molecular tools have created useful platforms enabling high-contrast or low-background RNA imaging.[7] A prominent approach is light-up RNA aptamers that can specifically bind and turn on nonfluorescent small-molecule dyes.[8−12] Target RNA can be genetically engineered with light-up RNA tags and tracked through activated fluorescence signals from the dye-aptamer complexes.[8−12] Direct imaging of endogenous RNAs has been achieved using genetically engineered RNA sensors based on split or structure-switched light-up RNAs.[13−15] An intrinsic limitation of light-up RNA approaches is that the dyes are not genetically encoded, requiring exogenous additions for RNA imaging.[16] Very recently, a new concept of RNA aptamer stabilized fluorogenic protein has been developed using fluorescent proteins fused with a Tat peptide-based degron.[17] The degron-fused fluorescent proteins are rapidly degraded, but become stabilized and fluorescent when the degron binds to a Tat peptide-binding RNA aptamer (called "Pepper" due to its multicolor fluorescence). This fluorogenic protein strategy is completely genetically encoded, resolving the issue with light-up RNA approaches. However, the fluorogenic protein strategy requires genetic engineering of target RNAs via inserting degron-binding RNA motifs.[16] Development of fluorogenic protein approaches for direct imaging of endogenous RNAs remains elusive.

Here we developed a new genetically encoded sensor using conformation-switching induced fluorogenic protein (csiFP), which enables direct imaging of endogenous RNAs. Because degradation of fluorogenic proteins was controlled by the degron-binding RNA aptamer (degApt) or Pepper,[17] we considered modulating the aptamer structure using target endogenous RNAs. We speculated that misfolding the stem-loop conformation of degApt via sequence extension could abrogate its degron-binding ability. In the situation, target RNA hybridization can restore its active conformation to bind

Received: July 24, 2021
Published: August 25, 2021

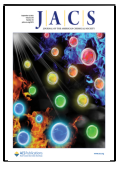

https://doi.org/10.1021/jacs.1c07719
J. Am. Chem. Soc. 2021, 143, 14394−14401

the degron, protecting the degron-fused fluorescent proteins from degradation.

Motivated by this hypothesis, we engineered the csiFP sensor system with an RNA sensing module and a degron-fused fluorescent protein reporter. We showed that target RNA could restore active conformation of degApt in the RNA sensing module, affording stabilized fluorescent proteins for target RNA imaging. We expanded the color palette of the sensor system and obtained four high-contrast csiFPs of distinct colors. The sensor was further extended using the split GFP design to afford highly sensitive signal amplifier for single molecule detection. We demonstrated the ability of the csiFP sensor for imaging the expression and dynamics of *survivin* mRNA and lncRNA MALAT-1 in live mammalian cells. We envision that this sensor can be broadly useful for RNA imaging in biomedical research and clinical theranostics.

RESULTS AND DISCUSSION

Design and In Vitro Characterization of csiFP Sensor. The csiFP sensor was designed to comprise two modules, an RNA sensing module and a degron-fused fluorescent protein reporter (Figure 1A). To control the degradation of fluorogenic proteins, we used degApt to construct the RNA sensing module and explored modulating its conformation using target RNA. The degApt exhibited a stem−loop conformation, and its stem region was crucial for binding a Tat peptide derived degron domain (tDeg).[17] Hence, we designed the RNA sensing module by extending degApt with a target RNA responsive sequence to disrupt its active conformation. This design could abrogate its binding ability to the tDeg-fused fluorescent protein reporter, resulting in rapid degradation of the protein with a low fluorescence background. Hybridization with target RNA mediated conformational switching of the RNA sensing module and restored active structure of degApt. Consequently, active degApt would bind the tDeg-fused fluorescent protein, shielding the degron from recruiting proteasomal machinery for proteolysis of the fusion proteins. In this way, target RNAs induced stabilization of fluorogenic RNA−protein complexes, delivering activated fluorescent signals for imaging.

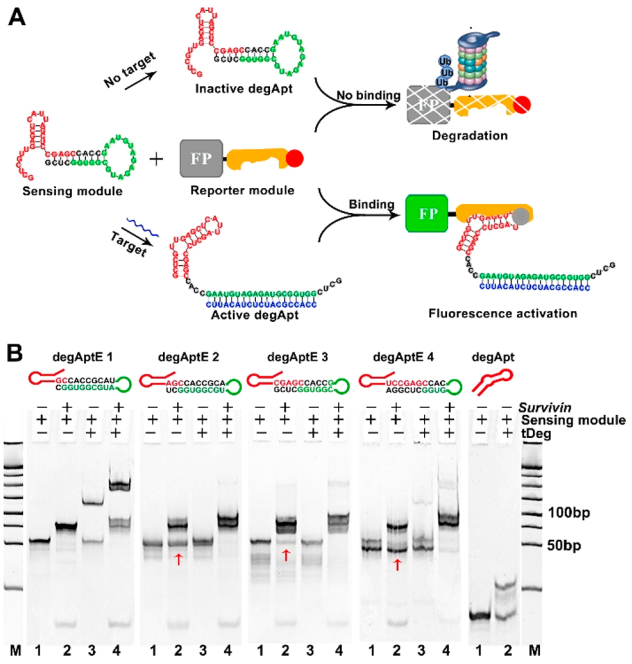

Figure 1. Design and in vitro characterization of csiFP sensor. (A) Schematic drawing of the csiFP sensor. (B) PAGE gel (20%) electrophoresis of degAptE 1−4 and degApt. Arrows indicated the remaining sensing module after hybridization with *survivin*. M denoted molecular weight marker. Representative data from three independent experiments.

We chose *survivin*, an mRNA overexpressed in various human cancer cells,[18,19] to demonstrate the approach. To construct the RNA sensing module, we extended degApt using a *survivin*-responsive sequence to disrupt the active conformation of degApt. A set of variants, degAptE 1−4, were designed with the extensions having different numbers of nucleotides complementary to the stem region of degApt. According to the mobility shifts in polyacrylamide gel electrophoresis (PAGE) analysis (Figure 1B), we found that variants degAptE 2, 3, and 4 showed negligible binding to the synthetic tDeg peptide, whereas degApt and degAptE 1 exhibited substantial binding affinity. After hybridization with RNA oligonucleotides of *survivin* mRNA, variant degAptE 3 recovered its ability to bind the degron. In contrast, degAptE 2 and 4 exhibited less hybridization efficiency with *survivin*, resulting in a smaller fraction of variants with restored degron-binding affinity. Together, we obtained variant degAptE 3 as the optimal RNA sensing module. In addition, variant degAptE 3 displayed no interactions for other RNA oligonucleotides of c-Myc, GalNac-7, and TK1 mRNAs (Figure S1 of the Supporting Information, SI), and showed negligible binding toward tDeg peptide even in large excess (Figure S2). This result suggested high specificity of degAptE 3 in response to *survivin* target.

Genetically Encoded csiFP Sensor for *Survivin* in Live Cells. To develop a genetically encoded csiFP sensor for *survivin* in mammalian cells, we engineered the RNA sensing module degAptE 3 in a circular RNA scaffold with the degron-fused EGFP reporter, EGFP-tDeg (Figure 2A). The circular RNA scaffold was constructed using the Tornado system, which utilized a ribozyme assisted circularization system, for high expression of the RNA sensing module in mammalian cells.[20] Two plasmids were constructed, a scaffolded degAptE 3 plasmid using a U6 promoter for expression of circular RNA degAptE 3 and an SV40 promoter for expression of iRFP transfection indicator, and a miniCMV promoter plasmid for expression of EGFP-tDeg (Figures S3 and S4).

We then evaluated whether the developed csiFP sensor enabled specific imaging of *survivin* in mammalian cells. After transfection with the EGFP-tDeg plasmid into MCF-7 cells, a cancer cell line with positive *survivin* expression,[18] negligible fluorescence for EGFP was detected (Figures 2B and S5). The fluorescence of EGFP was recovered after incubating the cells with MG132 (a proteasome inhibitor), suggesting that EGFP-tDeg was efficiently degraded via the proteasomal pathway. In contrast, MCF-7 cells cotransfected with EGFP-tDeg and scaffolded degAptE 3 plasmids displayed bright EGPF fluorescence with 22-fold enhancement. Further control assays were performed using NIH 3T3 cells, a mouse embryonic fibroblast cell line with negative human *survivin*.[18] After cotransfection using the EGFP-tDeg and scaffolded degAptE 3 plasmids, NIH 3T3 cells displayed negligible background signals of EGFP fluorescence, but strong EGFP fluorescence appeared after transfection of a human *survivin*-expressing plasmid. These results demonstrated that scaffolded degAptE 3

https://doi.org/10.1021/jacs.1c07719
J. Am. Chem. Soc. 2021, 143, 14394−14401

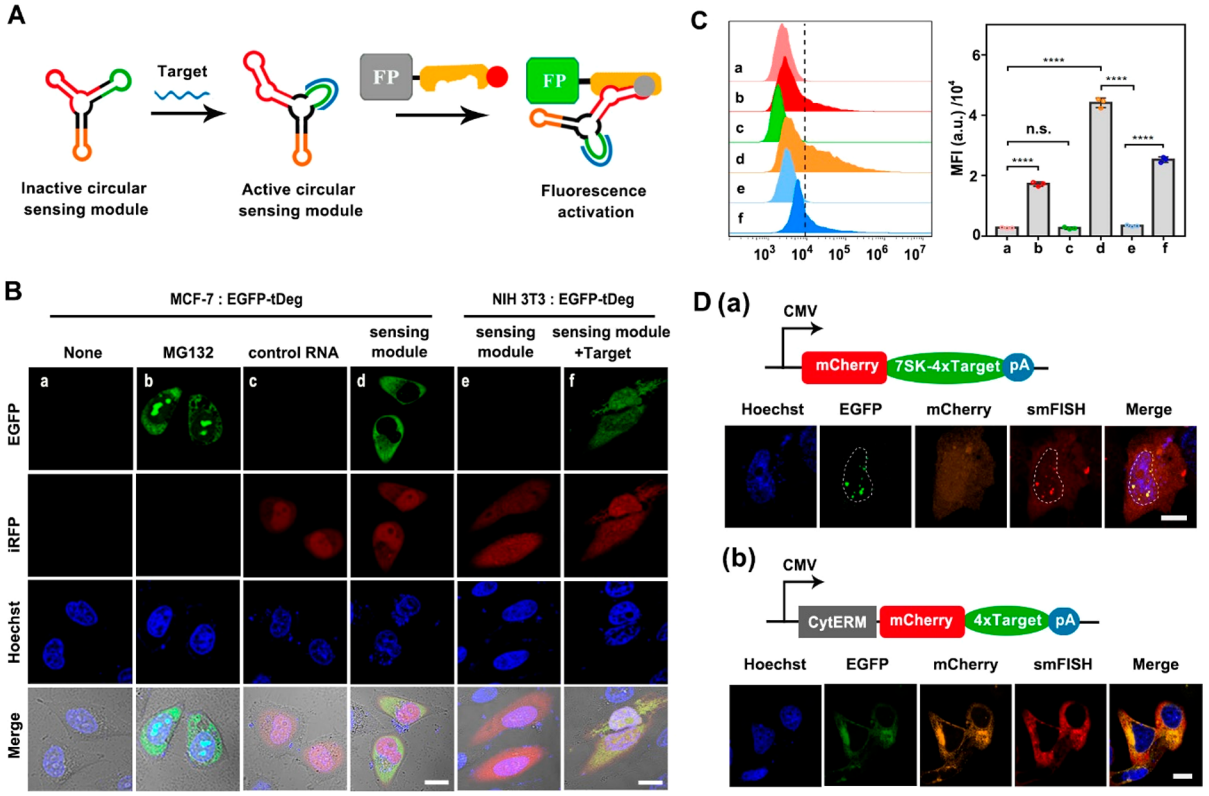

Figure 2. Genetically encoded csiFP sensor for *survivin* mRNA in live cells. (A) Schematic diagram for the working principle of csiFP sensor supported by a circular RNA scaffold using the Tornado system. (B) Fluorescence images for MCF-7 cells expressing EGFP-tDeg with none (a), 10 μM MG132 (b), circular RNA scaffolded control RNA (c) or circular RNA scaffolded degAptE 3 (d), and NIH 3T3 cells expressing EGFP-tDeg and circular RNA scaffolded degAptE 3 without (e) or with (f) target plasmid. (C) Flow cytometry profiles of the corresponding cells from three independent experiments and quantitative analysis. MFI: Mean fluorescence intensity. Statistical comparison was performed by two-tailed ŧtest, ****$p < 0.0001$, **$p < 0.01$, *$p < 0.05$, n.s., not significant. (D) Coexpression of csiFP sensor plasmids with tagged target RNA sequence, located in (a) nuclear or ER (b). Dashed circle indicated the nucleus region. (B, D) Representative data from three independent experiments. Scale bar: 10 μm.

could restore active conformation in response to *survivin* to protect EGFP-tDeg from degradation. Moreover, we observed very low EGFP fluorescence in MCF-7 cells transfected with EGFP-tDeg and a control RNA sensing module with mutations in the *survivin*-complementary sequence. An additional control using MCF-7 cells with *survivin* knocked down by small interference RNA (siRNA), as confirmed by qRT-PCR (Figure S6), showed remarkably decreased EGFP fluorescence. This observation suggested that specific hybridization of *survivin* mRNA with degAptE 3 was essential for the stabilization of EGFP-tDeg. A further flow cytometry analysis of the MCF-7 and NIH 3T3 cells also confirmed the ability of csiFP sensor for specific detection of *survivin* (Figure 2C). In addition, time-dependent imaging revealed that EGFP fluorescence appeared at 2 h post-transfection followed by gradual increase until saturation after 10 h through 72 h (Figure S7).

We also investigated the effects of the RNA scaffold using degAptE 3 in a $tRNA_{lys}$ scaffold or without a scaffold. It was found that the tRNA scaffolded degAptE 3 gave slightly decreased EGFP fluorescence, while degAptE 3 without a scaffold only showed very weak EGFP fluorescence (Figure S8). These results indicated that scaffold systems were critical for stable expression of degAptE 3 in mammalian cells, and circular scaffolds conferred improved signal-to-background ratio. Thus, the Tornado system was used for the RNA sensing module in subsequent assays. Moreover, a positive control using an "always-on" aptamer degApt within the Tornado system showed intense fluorescence in the cytoplasm with remarkable fluorescent dots in the nucleus (Figure S9), evidencing nucleus-localized artifacts from the "always-on" Tornado system, consistent with previous reports.[20,21] Interestingly, we observed no fluorescent signals in the nucleus and cytoplasm for degAptE 3 within the Tornado system in the negative NIH 3T3 cells, and for the control RNA sensing module in the positive MCF-7 and HeLa cells. This result implied that the target-responsive design of csiFP sensor offered an advantage over the "always-on" Tornado system in avoiding nucleus-localized artifacts.

Surprisingly, a Z-stacked imaging analysis of MCF-7 cells showed that csiFP sensor gave EGFP fluorescence predominantly distributed in the cytoplasm with a few remarkable fluorescent dots in the nucleus (Figure S10). The localization of *survivin* mRNA was further verified using single-molecule fluorescence in situ hybridization (smFISH), which displayed colocalized fluorescence signals with those obtained with csiFP sensor (Figure S11). A closer interrogation was performed by expressing a target sequence inserted nucleus-localized 7SK small nuclear RNA or an endoplasmic reticulum-localized mRNA[12] in NIH 3T3 cells (Figure S12). As anticipated, we observed colocalization of EGFP fluorescence with nucleus and endoplasmic reticulum (Figure 2D). Moreover, the EGFP fluorescence signals colocalized with those from smFISH of mCherry mRNA with Pearson's correlation coefficients

https://doi.org/10.1021/jacs.1c07719
J. Am. Chem. Soc. 2021, 143, 14394−14401

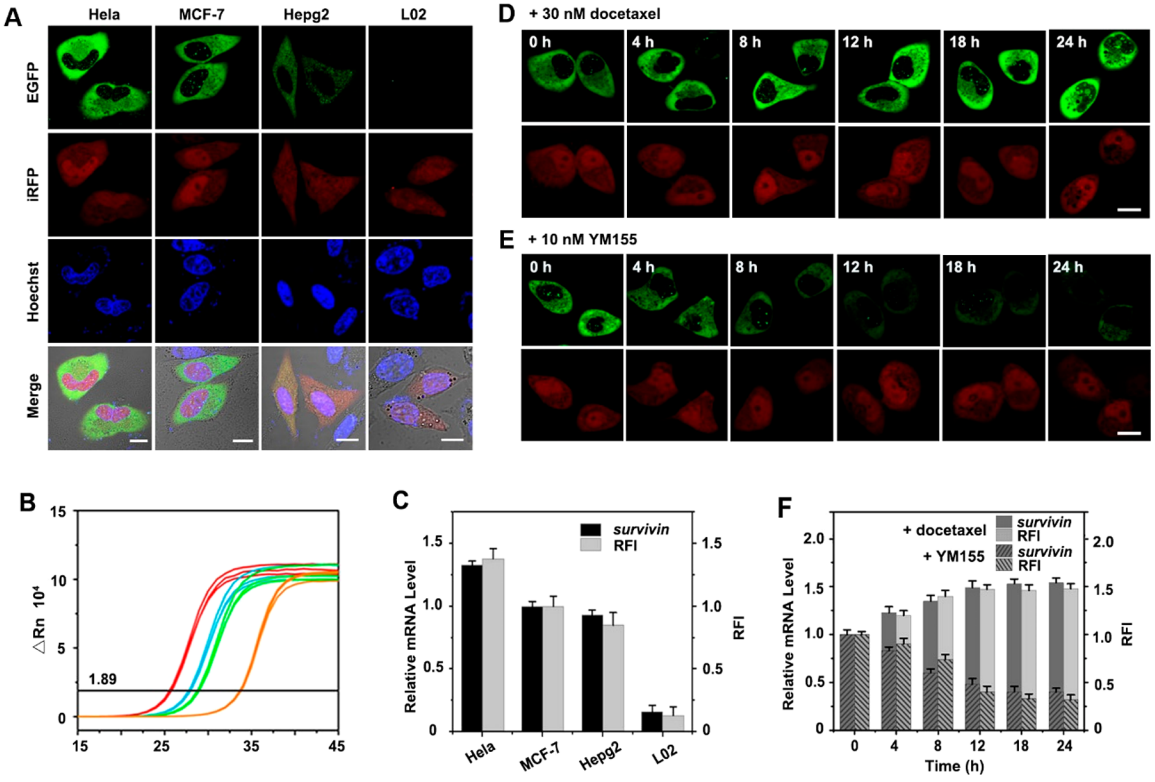

Figure 3. (A) Fluorescence images for different cells expressing csiFP sensor. (B) qRT-PCR data for the cells from three independent experiments. Red: HeLa, cyan: MCF-7, green: Hepg2, orange: L02. (C) Relative expression levels of *survivin* mRNA and relative fluorescence intensity (RFI) in different cells. Relative expression levels of *survivin* determined using GAPDH as a control and were represented as mean ± s.d. from three different experiments. RFI data was shown as mean ± s.d. (HeLa, n = 30; MCF-7, n = 52; Hepg2, n = 28; L02, n = 25). Real-time fluorescence images of MCF-7 cells with 30 nM docetaxel (D) or 10 nM YM155 (E) after 12 h of transfection with the csiFP sensor encoding plasmids. (F) Relative expression levels of *survivin* mRNA and RFI in different treated times. Relative expression levels of *survivin* determined using GAPDH as a control and were represented as mean ± s.d. RFI data was shown as mean ± s.d. (n = 45). (A, D, E) Representative data from three independent experiments. Scale bar: 10 μm.

(PCCs) of 0.86 and 0.76 for the nucleus and endoplasmic reticulum localized mRNAs, respectively. Together, these results suggested that our csiFP sensor did not affect subcellular localization of target RNA.

csiFP Sensor for Live-Cell *Survivin* Imaging. We then employed the csiFP sensor to image *survivin* in different cell lines with varying expression levels. We found that HeLa cells delivered the most intense fluorescence whereas L02 cells showed negligible EGFP signal, and MCF-7 cells exhibited stronger EGFP fluorescence than HepG2 cells (Figure 3A). These results indicated that HeLa, MCF-7, HepG2, and L02 cells had decreasing *survivin* expression, consistent with previous reports.[18,19] Moreover, the average EGFP fluorescence intensity in more than 20 cells were in good agreement with the relative concentrations of *survivin* mRNA determined by qRT-PCR (Figure 3B,C). This result verified that our csiFP sensor was capable of quantifying relative *survivin* mRNA abundance in live cells. Furthermore, the csiFP sensor was investigated for imaging HeLa and MCF-7 cells treated with docetaxel (*survivin* inducer) or YM155 (*survivin* inhibitor).[19] It was reported that the expression level of *survivin* mRNA ranged from moderate abundance (~300 copies/cell) to high abundance (>5000 copies/cell) in these drug-treated cells.[19] As anticipated, cells induced with docetaxel showed brighter EGFP fluorescence whereas those treated with YM155 delivered lower EGFP fluorescence (Figure S13). Moreover, higher doses of docetaxel led to stronger EGFP fluorescence whereas higher doses of YM155 displayed decreasing EGFP signals. The fluorescence signals were dynamically correlated to the relative *survivin* concentrations, as determined by qRT-PCR. These results revealed the capability of our csiFP sensor for quantitative imaging of *survivin* mRNA with moderate to high abundance in live cells. We further examined the ability of the csiFP sensor to monitor the dynamics of *survivin* in response to drug treatments. After transfection with the csiFP sensor, MCF-7 cells treated with docetaxel or YM155 were monitored for 24 h. We observed almost constant EGFP fluorescence in cells without drug treatment (Figure S14). Upon treatment of the cells with docetaxel, EGFP fluorescence became gradually increasing until stabilization at ~8 h (Figure 3D). After stimulation with YM155, the cells delivered gradually decreased EGFP fluorescence until stabilization at ~18 h (Figure 3E). The fluorescence changes were in good agreement with *survivin* expressions as determined by qRT-PCR assays (Figures 3F and S15). A control experiment using the "always-on" RNA aptamer degApt in place of the sensing module showed steady bright EGFP fluorescence in cells under different drug treatments (Figure S16). Additionally, the transfection indicator iRFP also exhibited consistent fluorescence through the drug-treated cells. Both controls confirmed that the drug treatment had little effect on the turnover of fluorescent proteins. Together, these results revealed that our csiFP sensor enabled continuous imaging of the dynamics of *survivin* expression.

https://doi.org/10.1021/jacs.1c07719
J. Am. Chem. Soc. 2021, 143, 14394−14401

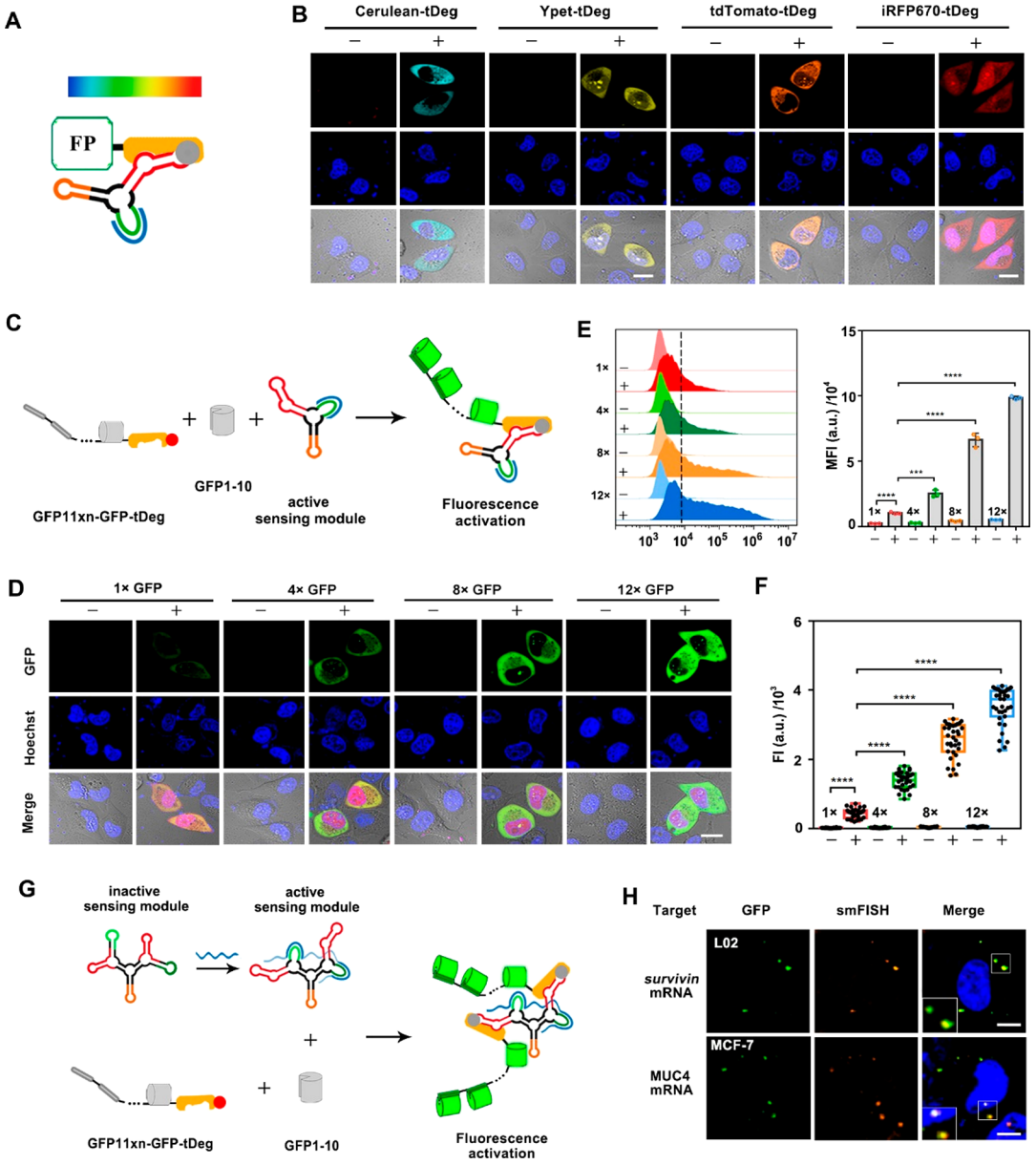

Figure 4. Engineering of multicolor sensor and csiFP signal amplifier. (A) Schematic of multicolor csiFP sensor. (B) Fluorescence images for cells transfection with various FP-tDeg, "−": none, "+": circular sensor responsive to *survivin*. (C) Schematic of fluorescence signal amplification by GFP-tDeg fusion tagged with a GFP11 tandem. (D) Fluorescence images for MCF-7 cells expressing csiFP sensors with varying signal amplifiers. (E) Flow cytometry profiles of the corresponding cells from three independent experiments and quantitative analysis. (F) Quantitative analysis of corresponding FI in individual cells. Data were represented as mean ± s.d. (n = 52). (G) Schematic of 24× csiFP amplifier for target mRNA. (H) Fluorescence images of *survivin* mRNA in L02 cells and MUC4 mRNA in MCF7 cells using 24× csiFP amplifier and colocalization with the corresponding smFISH probes. Statistical comparison was performed by two-tailed ŧtest, ****p < 0.0001, ***p < 0.001. (B, D, H) Representative data from three independent experiments. Scale bar: 10 μm.

Engineering of Multicolor Sensor and csiFP Signal Amplifier. To expand the color palette of csiFP sensor for multicolor imaging applications, we explored the possibility of using fluorescent proteins with distinct colors as the reporter (Figure 4A). In initial trials, we examined mCherry and iRFP713 with orange and NIR fluorescence. Surprisingly, very low mCherry or iRFP713 fluorescence was found in MCF-7 cells transfected using plasmids expressing scaffolded degAptE 3 together with mCherry-tDeg or iRFP713-tDeg (Figure S17). In contrast, substitution of degAptE 3 by degApt resulted in intense fluorescence. This finding suggested that mCherry-tDeg and iRFP713-tDeg could still be protected by the degron-binding aptamer degApt, but *survivin* hybridization with degAptE 3 could not effectively prevent the degradation. We ascribed the inadequate protection efficiency for mCherry-tDeg and iRFP713-tDeg to their intrinsic fast degradation rates.

To develop a multicolor palette for csiFP sensor, we endeavored to screen fluorescent proteins with possibly varying degradation properties, including Cerulean, Ypet, tdTomato, mRuby2, mKO, mKO2, iRFP670, miRFP703, mIFP, and PAiRFP1 (Table S3).[22,23] These tDeg-fused fluorescence proteins all displayed low fluorescence, indicating their efficient degradation in MCF-7 cells. To our delight, MCF-7 cells

https://doi.org/10.1021/jacs.1c07719
J. Am. Chem. Soc. 2021, 143, 14394−14401

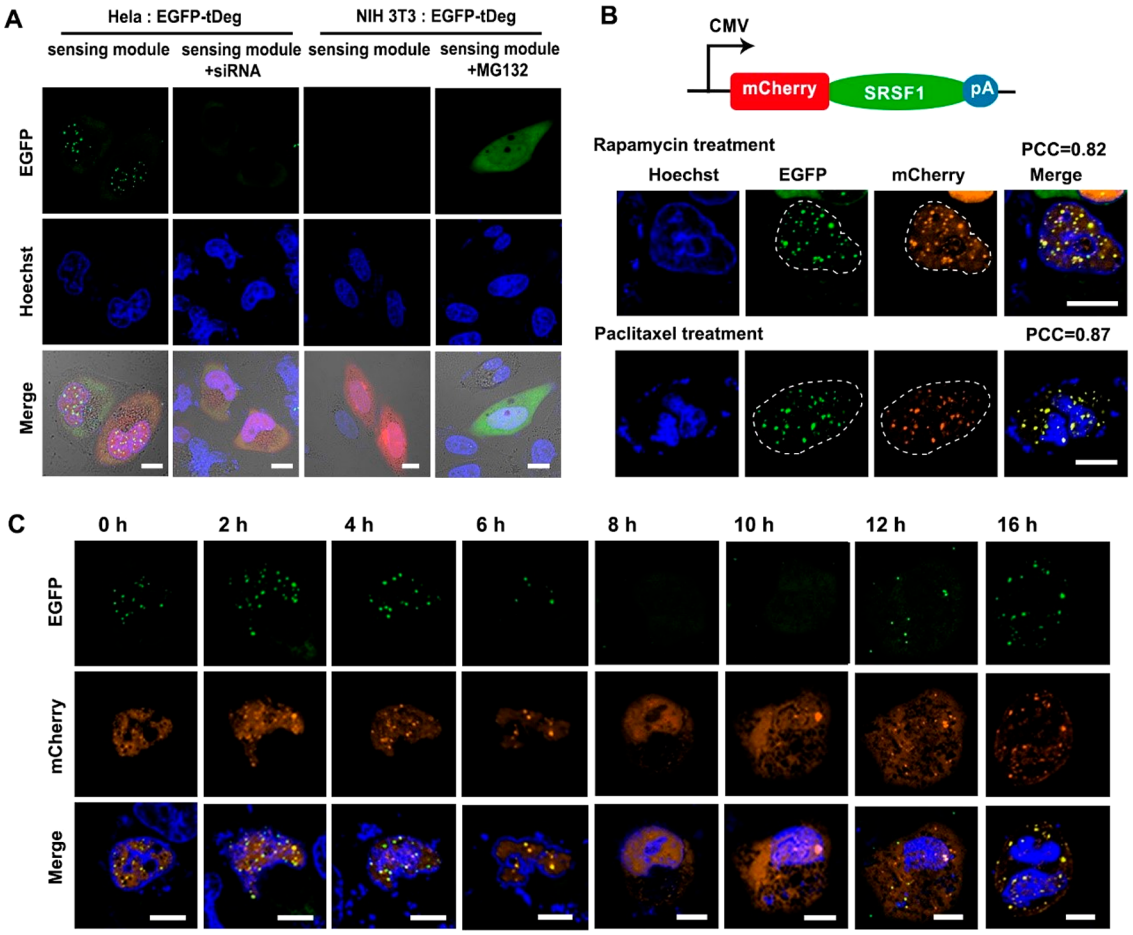

Figure 5. csiFP sensor for lncRNA MALAT-1 imaging. (A) Fluorescence images for HeLa and NIH 3T3 cells expressing csiFP sensor for lncRNA MALAT-1. (B) Fluorescence images for HeLa cells transfection csiFP sensor for lncRNA MALAT-1 with mCherry-SRSF1 plamids. S phase: cells treated 0.1 μM rapamycin for 24 h, M phase: cells treated 0.1 μM paclitaxel for 16 h. (C) Real-time fluorescence imaging for HeLa cells expressing csiFP sensor for lncRNA MALAT-1. Representative data from three independent experiments. Scale bar: 10 μm.

cotransfected with scaffolded degAptE 3 and several tDeg-fused fluorescent proteins, Cerulean, Ypet, tdTomato, mKO2, iRFP670, and miRF703, exhibited fluorescence signals with high signal-to-background ratios (Figures 4B and S18). Surprisingly, mKO, a protein with three more lysine residues than mKO2,[23] showed much lower fluorescence than mKO2. Presumably, this distinction was attributed to the faster degradation rate of mKO with more lysine residues. Other fluorescent proteins such as mRuby2 and mIFP also delivered low fluorescence. Together, combining protein reporters of Cerulean, Ypet, tdTomato, mKO2, iRFP670, and miRF703, we accomplished fine-tuning of the csiFP sensor color palette in the emission color range from blue to NIR. Protein reporters, Cerulean, EGFP, tdTomato, and iRFP670, afforded four channels without spectral crosstalk for multicolor fluorescence imaging.

We then inspected the possibility of developing signal amplifier of csiFP sensors. Signal amplification of csiFP sensors could be directly achieved by using a tandem of fluorescent proteins. However, fusion of fluorescent proteins with >3 copies was challenging due to bacterial recombination in plasmid construction.[17] We engineered a signal amplifier of csiFP sensor using the split GFP system (Figure 4C).[24] The system comprised two nonfluorescent parts, GFP1-10 (a large fragment consisting of the 1st to the 10th β-strands) and GFP 11 (the 11th β-strand with 16 amino acids), which could be reconstituted to generate fluorescent GFP. We constructed a plasmid GFP11-tDeg with two cassettes, one for expressing GFP-tDeg fusion tagged with a tandem array of GFP11 and the other for expressing GFP1-10 (Figures 4C and S19). As anticipated, these csiFP sensors with varying signal amplifiers (from 1× to 12×) displayed increasing GFP fluorescence in MCF-7 cells as the tandem repeats increased (Figures 4D,F and S20). Flow cytometry assay also confirmed enhanced fluorescence signal-to-background (S/B) ratios (5-, 9-, 15-, and 19-fold) for varying signal amplifiers (1×, 4×, 8×, and 12×) (Figure 4E). This result validated the ability of the csiFP signal amplifier to enhance the contrast or S/B ratio for mRNA detection and imaging. The potential of the csiFP amplifier for single-molecule imaging was further investigated. To achieve adequate sensitivity, we developed a csiFP amplifier using a circular RNA that comprised two sensing modules responsive to proximal regions of target RNA (Figure 4G), resulting in a double 12× signal amplifier (24× signal amplifier). Two csiFP sensors were designed for single-molecule imaging of two low-abundance mRNAs, *survivin* mRNA in L02 cells and MUC4 mRNA in MCF-7 cells.[25] As anticipated, we observed GFP fluorescence puncta in L02 cells for *survivin* imaging and in MCF-7 cells for MUC4 imaging (Figure 4H). Further smFISH assays gave fluorescence puncta which were colocalized with those from the corresponding 24× csiFP amplifier. The PCCs were estimated to be 0.85 and 0.83 for *survivin* and MUC4,

https://doi.org/10.1021/jacs.1c07719
J. Am. Chem. Soc. 2021, 143, 14394−14401

respectively. In addition, the specificity of two csiFP amplifiers was testified via knockdown of *survivin* and MUC4 mRNAs with the corresponding siRNAs (Figure S21). Together, these results demonstrated the capability of our csiFP amplifier for detecting target mRNA at the single molecule level.

csiFP Sensor for lncRNA MALAT-1 Imaging. To demonstrate the generality of our csiFP sensor for imaging other RNA in live cells, we engineered a csiFP sensor for human MALAT-1, a lncRNA involved in tumor growth and metastasis and overexpressed in many cancers.[26,27] A sensing module for MALAT-1 was designed by replacing the *survivin*-responsive region with MALAT-1 complementary sequence. We found that the csiFP sensor for MALAT-1 exhibited bright EGFP fluorescence in HeLa cells (Figure 5A). By contrast, a mouse embryonic fibroblast cell line NIH3T3 with no human MALAT-1 expression delivered negligible EGFP fluorescence. A control experiment with NIH3T3 cells pretreated the proteasome inhibitor MG132 showed intense EGFP fluorescence, indicating positive expression of EGFP-tDeg in the cells. Moreover, HeLa cells depleted with MALAT-1 via siRNA displayed remarkably reduced EGFP fluorescence. Additional qRT-PCR confirmed the knockdown of MALAT-1 (Figure S22). These results verified that the csiFP sensor allowed specific detection of MALAT-1 in living cells.

Next, we investigated subcellular localization dynamics of MALAT-1 in the cells (Figure 5B). MALAT-1 was reported to be predominantly localized in nuclear speckles in interphase cells and concentrated in mitotic interchromatin granules clusters (IGCs) in mitotic cells.[26] HeLa cells were synchronized in interphase (S phase) by treatment with rapamycin,[27] as confirmed by flow cytometry analysis using propidium iodide (PI) staining (Figure S23). We found that the csiFP sensor with EGFP-tDeg reporter exhibited predominant localization in the nuclei with speckled fluorescence. A further assay with a mCherry-fused nuclear speckle marker protein serine/arginine-rich splicing factor 1 (mCherry-SRSF1) showed colocalization of MALAT-1 with SRSF1 (Figure 5B). The PCCs between fluorescence signals of EGFP and mCherry for cells treated with rapamycin and paclitaxel were 0.82 and 0.87, respectively. A Z-stacked imaging analysis further confirmed the colocalization of MALAT-1 with SRSF1 (Figure S24). This finding clearly illustrated the predominant nuclear speckle localization of MALAT-1 in interphase cells, consistent with literature reports.[26] This result indicated that the csiFP sensor was capable of detecting endogenous nucleus-localized RNA with no perturbation to its localization. After HeLa cells were induced with paclitaxel to undergo mitosis, the EGFP fluorescence became dispersed in the cytoplasm after breakdown of the nuclear envelop. A colocalization assay with mCherry-SRSF1 and Z-stack imaging analysis showed that MALAT-1 remained localized in proximity to SRSF1 (Figures 5B and S25). A time-dependent imaging of MALAT-1 during mitosis induction revealed that EGFP fluorescence puncta, together with the SRSF1 puncta, first became diffusely distributed throughout the cytoplasm owing to nuclear envelop breakdown, and then concentrated into bright foci in the cytosol due to the IGCs formation (Figures 5C). This result revealed the dynamic translocation of MALAT-1 during mitosis, which was consistent with the disassembly and cytosolic dispersion process of nuclear speckles upon mitosis induction.[28] This result demonstrated that our csiFP sensor was capable of imaging and tracking the translocation of endogenous lncRNA in live cells.

In addition, the csiFP sensor using NIR fluorescence protein reporter iRFP670 also showed predominant nuclear speckle localization of MALAT-1 in interphase cells and became dispersed into the cytoplasm during mitosis (Figure S26). The 12× signal amplifier displayed consistent results with higher contrast. These results demonstrated the potential of the csiFP sensor for high-contrast imaging of MALAT-1.

CONCLUSIONS

We developed a new genetically encoded csiFP sensor for live cell imaging of endogenous RNA expression and dynamics. We demonstrated that a designed misfolding degron-binding aptamer could restore active conformation upon target RNA hybridization, stabilizing the degron-fused protein for fluorogenic imaging. By incorporating the misfolding aptamer in a circular RNA scaffold, a genetically encoded csiFP sensor was engineered that enabled quantitative and continuous *survivin* imaging in mammalian cells. We expanded the color palette of csiFP sensor to the whole emission range from blue to NIR, which could afford the potential for multicolor and in vivo imaging. Signal amplifiers of csiFP sensors were further developed using the split fluorescent protein system, enabling live cell imaging of RNA with very low-abundance at the single molecule level. The csiFP sensor was applied for imaging and tracking lncRNA MALAT-1 in live cells, revealing that MALAT-1 localized in nuclear speckles in interphase cells and became dispersed in the nuclei and cytoplasm during mitosis. Our strategy could provide a new paradigm for highly sensitive, multicolor imaging of endogenous RNA in live cells and animals.

ASSOCIATED CONTENT

Supporting Information

The Supporting Information is available free of charge at https://pubs.acs.org/doi/10.1021/jacs.1c07719.

Experimental details for plasmid construction, gel electrophoresis, cell culture, transfection and imaging, smFISH, flow cytometry, qRT-PCR, and additional figures (PDF)

AUTHOR INFORMATION

Corresponding Authors

Fenglin Wang − *State Key Laboratory of Chemo/Biosensing and Chemometrics, College of Chemistry and Chemical Engineering, Hunan University, Changsha 410082, P. R. China*; orcid.org/0000-0002-5872-2693; Email: fengliw@hnu.edu.cn

Jian-Hui Jiang − *State Key Laboratory of Chemo/Biosensing and Chemometrics, College of Chemistry and Chemical Engineering, Hunan University, Changsha 410082, P. R. China*; orcid.org/0000-0003-1594-4023; Email: jianhuijiang@hnu.edu.cn

Authors

Wen-Jing Zhou − *State Key Laboratory of Chemo/Biosensing and Chemometrics, College of Chemistry and Chemical Engineering, Hunan University, Changsha 410082, P. R. China*

Hua Li − *State Key Laboratory of Chemo/Biosensing and Chemometrics, College of Chemistry and Chemical*

Engineering, Hunan University, Changsha 410082, P. R. China

Ke-Ke Zhang − *State Key Laboratory of Chemo/Biosensing and Chemometrics, College of Chemistry and Chemical Engineering, Hunan University, Changsha 410082, P. R. China*

Xia Chu − *State Key Laboratory of Chemo/Biosensing and Chemometrics, College of Chemistry and Chemical Engineering, Hunan University, Changsha 410082, P. R. China;* orcid.org/0000-0002-4120-6131

Complete contact information is available at: https://pubs.acs.org/10.1021/jacs.1c07719

Author Contributions

The manuscript was written through contributions of all authors. All authors have given approval to the final version of the manuscript.

Notes

The authors declare no competing financial interest.

■ ACKNOWLEDGMENTS

This work was supported by National Key Research Program (2019YFA0905800, 2018YFA0902300) and National Natural Science Foundation of China (22090050, 21991080, 21904034).

■ REFERENCES

(1) Wolin, S. L.; Maquat, L. E. Cellular RNA surveillance in health and disease. *Science* **2019**, *366* (6467), 822−827.

(2) Tutucci, E.; Vera, M.; Biswas, J.; Garcia, J.; Parker, R.; Singer, R. H. An improved MS2 system for accurate reporting of the mRNA life cycle. *Nat. Methods* **2018**, *15* (1), 81−89.

(3) Tanenbaum, M. E.; Gilbert, L. A.; Qi, L. S.; Weissman, J. S.; Vale, R. D. A protein-tagging system for signal amplification in gene expression and fluorescence imaging. *Cell* **2014**, *159* (3), 635−646.

(4) Xu, W.; He, W.; Du, Z.; Zhu, L.; Huang, K.; Lu, Y.; Luo, Y. Functional nucleic acid nanomaterials: development, properties, and applications. *Angew. Chem., Int. Ed.* **2021**, *60* (13), 6890−6918.

(5) Navani, N. K.; Li, Y. Nucleic acid aptamers and enzymes as sensors. *Curr. Opin. Chem. Biol.* **2006**, *10* (3), 272−281.

(6) Briley, W. E.; Bondy, M. H.; Randeria, P. S.; Dupper, T. J.; Mirkin, C. A. Quantification and real-time tracking of RNA in live cells using Sticky-flares. *Proc. Natl. Acad. Sci. U. S. A.* **2015**, *112* (31), 9591−9595.

(7) Pichon, X.; Lagha, M.; Mueller, F.; Bertrand, E. A growing toolbox to image gene expression in single cells: sensitive approaches for demanding challenges. *Mol. Cell* **2018**, *71* (3), 468−480.

(8) Li, X.; Kim, H.; Litke, J. L.; Wu, J.; Jaffrey, S. R. Fluorophore-promoted RNA folding and photostability enables imaging of single Broccoli-tagged mRNAs in live mammalian cells. *Angew. Chem., Int. Ed.* **2020**, *59* (11), 4511−4518.

(9) Cawte, A. D.; Unrau, P. J.; Rueda, D. S. Live cell imaging of single RNA molecules with fluorogenic Mango II arrays. *Nat. Commun.* **2020**, *11* (1), 1283.

(10) Bouhedda, F.; Fam, K. T.; Collot, M.; Autour, A.; Marzi, S.; Klymchenko, A.; Ryckelynck, M. A dimerization-based fluorogenic dye-aptamer module for RNA imaging in live cells. *Nat. Chem. Biol.* **2020**, *16* (1), 69−76.

(11) Su, Y.; Hammond, M. C. RNA-based fluorescent biosensors for live cell imaging of small molecules and RNAs. *Curr. Opin. Biotechnol.* **2020**, *63*, 157−166.

(12) Chen, X.; Zhang, D.; Su, N.; Bao, B.; Xie, X.; Zuo, F.; Yang, L.; Wang, H.; Jiang, L.; Lin, Q.; Fang, M.; Li, N.; Hua, X.; Chen, Z.; Bao, C.; Xu, J.; Du, W.; Zhang, L.; Zhao, Y.; Zhu, L.; Loscalzo, J.; Yang, Y. Visualizing RNA dynamics in live cells with bright and stable fluorescent RNAs. *Nat. Biotechnol.* **2019**, *37*, 1287−1293.

(13) Wang, Z.; Luo, Y.; Xie, X.; Hu, X.; Song, H.; Zhao, Y.; Shi, J.; Wang, L.; Glinsky, G.; Chen, N.; Lal, R.; Fan, C. In situ spatial complementation of aptamer-mediated recognition enables live-cell imaging of native RNA transcripts in real time. *Angew. Chem.* **2018**, *130* (4), 984−988.

(14) Ying, Z. M.; Wu, Z.; Tu, B.; Tan, W.; Jiang, J. H. Genetically encoded fluorescent RNA sensor for ratiometric imaging of microRNA in living tumor cells. *J. Am. Chem. Soc.* **2017**, *139* (29), 9779−9782.

(15) Karunanayake Mudiyanselage, A.; Yu, Q.; Leon-Duque, M. A.; Zhao, B.; Wu, R.; You, M. Genetically encoded catalytic hairpin assembly for sensitive RNA imaging in live cells. *J. Am. Chem. Soc.* **2018**, *140* (28), 8739−8745.

(16) Wu, J.; Jaffrey, S. R. Imaging mRNA trafficking in living cells using fluorogenic proteins. *Curr. Opin. Chem. Biol.* **2020**, *57*, 177−183.

(17) Wu, J.; Zaccara, S.; Khuperkar, D.; Kim, H.; Tanenbaum, M. E.; Jaffrey, S. R. Live imaging of mRNA using RNA-stabilized fluorogenic proteins. *Nat. Methods* **2019**, *16* (9), 862−865.

(18) Peng, X.-H.; Cao, Z.-H.; Xia, J.-T.; Carlson, G. W.; Lewis, M. M.; Wood, W. C.; Yang, L. Real-time detection of gene expression in cancer cells using molecular beacon imaging: new strategies for cancer research. *Cancer Res.* **2005**, *65* (5), 1909−1917.

(19) Ying, Z. M.; Wang, F.; Chu, X.; Yu, R. Q.; Jiang, J. H. Activatable CRISPR transcriptional circuits generate functional RNA for mRNA sensing and silencing. *Angew. Chem., Int. Ed.* **2020**, *59* (42), 18599−18604.

(20) Litke, J. L.; Jaffrey, S. R. Highly efficient expression of circular RNA aptamers in cells using autocatalytic transcripts. *Nat. Biotechnol.* **2019**, *37* (6), 667−675.

(21) Sunbul, M.; Lackner, J.; Martin, A.; Englert, D.; Hacene, B.; Grun, F.; Nienhaus, K.; Nienhaus, G. U.; Jaschke, A. Super-resolution RNA imaging using a rhodamine-binding aptamer with fast exchange kinetics. *Nat. Biotechnol.* **2021**, *39* (6), 686−690.

(22) Shaner, N. C.; Steinbach, P. A.; Tsien, R. Y. A guide to choosing fluorescent proteins. *Nat. Methods* **2005**, *2* (12), 905−909.

(23) Sakaue-Sawano, A.; Kurokawa, H.; Morimura, T.; Hanyu, A.; Hama, H.; Osawa, H.; Kashiwagi, S.; Fukami, K.; Miyata, T.; Miyoshi, H.; Imamura, T.; Ogawa, M.; Masai, H.; Miyawaki, A. Visualizing spatiotemporal dynamics of multicellular cell-cycle progression. *Cell* **2008**, *132* (3), 487−98.

(24) Kamiyama, D.; Sekine, S.; Barsi-Rhyne, B.; Hu, J.; Chen, B.; Gilbert, L. A.; Ishikawa, H.; Leonetti, M. D.; Marshall, W. F.; Weissman, J. S.; Huang, B. Versatile protein tagging in cells with split fluorescent protein. *Nat. Commun.* **2016**, *7* (1), 11046.

(25) Yang, L. Z.; Wang, Y.; Li, S. Q.; Yao, R. W.; Luan, P. F.; Wu, H.; Carmichael, G. G.; Chen, L. L. Dynamic imaging of RNA in living cells by CRISPR-Cas13 systems. *Mol. Cell* **2019**, *76* (6), 981−997.

(26) Tripathi, V.; Ellis, J. D.; Shen, Z.; Song, D. Y.; Pan, Q.; Watt, A. T.; Freier, S. M.; Bennett, C. F.; Sharma, A.; Bubulya, P. A.; Blencowe, B. J.; Prasanth, S. G.; Prasanth, K. V. The nuclear-retained noncoding RNA MALAT1 regulates alternative splicing by modulating SR splicing factor phosphorylation. *Mol. Cell* **2010**, *39* (6), 925−938.

(27) Moreno-Torres, M.; Jaquenoud, M.; De Virgilio, C. TORC1 controls G1-S cell cycle transition in yeast via Mpk1 and the greatwall kinase pathway. *Nat. Commun.* **2015**, *6*, 8256.

(28) Lamond, A. I.; Spector, D. L. Nuclear speckles: a model for nuclear organelles. *Nat. Rev. Mol. Cell Biol.* **2003**, *4* (8), 605−12.